ACSNANO
www.acsnano.org
ARTICLE

Real-Space, *in Situ* Maps of Hydrogel Pores

Lingxiang Jiang[†] and Steve Granick*[,‡]

[†]Department of Materials Science and Engineering, Jinan University, Guangzhou 510632, China
[‡]IBS Center for Soft and Living Matter and UNIST, Ulsan 689-798, South Korea

Supporting Information

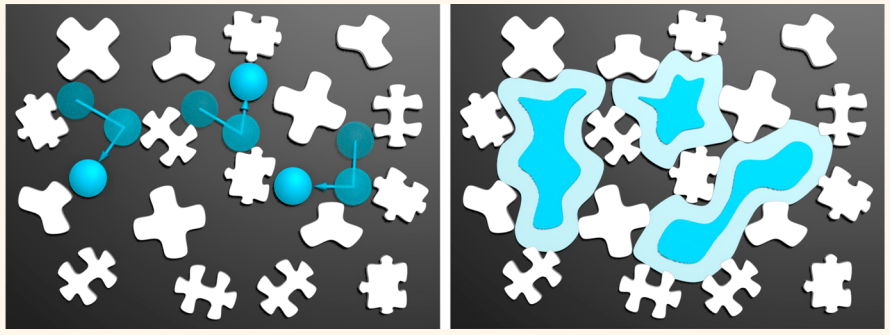

ABSTRACT: **We characterize the porosity of hydrogels by imaging the displacement trajectories of embedded tracer particles. This offers the possibility of characterizing the size and projected shape of individual pores as well as direct, real-space maps of heterogeneous porosity and its distribution. The scheme shows that when fluorescent spherical particles treated to avoid specific adsorption are loaded into the gel, their displacement trajectories from Brownian motion report on the size and projected shape in which the pore resides, convoluted by the particle size. Of special interest is how pores and their distribution respond to stimuli. These ideas are validated in agarose gels loaded with latex particles stabilized by adsorbed bovine serum albumin. Gels heated from room temperature produced an increasingly more monodisperse pore size distribution because increasing temperature preferentially enlarges smaller pores, but this was irreversible upon cooling, and shearing agarose gels beyond the yield point destroyed larger pores preferably. The method is considered to be generalizable beyond the agarose system presented here as proof of concept.**

KEYWORDS: *particle-tracking, hydrogel, porosity, stimuli-response*

When a porous microstructure changes with time and is massively heterogeneous, the standard methods to characterize porous gels have limited effectiveness.[1] For example, adsorption,[2] light/X-ray/neutron scattering,[3,4] fluorescence recovery,[5] and NMR[6] can discriminate neither real-space nor single-pore information, while microscopy is usually *post-mortem* and cannot follow pores whose sizes or shapes evolve in real time.[7−9] Our particular interest is porosity in hydrogels, but the generic limitation holds back progress in numerous applications, for example, transport and separation of small molecules, controlled release, cell culture, and tissue engineering.[10−14] Below, we argue the advantage of combining two communities that have evolved independently and with too little cross-talk:[15,16] the scientific communities of those interested in porosity characterization[1−9] and those interested in particle tracking.

The huge community that focuses on tracking particle trajectories in real-time and real-space usually by optical microscopy[17,18] and more recently by electron microscopy[19] has developed a number of applications including micro-rheology, where particles embedded in complex fluids are tracked to infer the local or overall viscoelastic properties.[20,21] Microrheology has been further extended to study hetero-geneity,[22] sol−gel transition,[23] stimuli responses,[24] *etc.* Inspired by this, here we describe methods to characterize porosity in real space and real time by incorporating trace particles into porous systems and tracking their trajectories. The needed expertise in particle tracking is widely available even for those without experitse in this specific subject,[25,26] therefore presenting a low barrier to implement these ideas.

As outlined schematically in Figure 1, the conceptual idea is to embed tiny tracer particles within the hydrogel such that the diffusion space that they explore maps the spatial makeup of the hydrogel pores. The hydrogel system selected for specific study consists of agarose fibers that, when cooled well below their clearing temperature of ∼90 °C, form a 3-dimensional, physically cross-linked framework with disordered, interconnecting pores swollen by water (Figure 1a). Into the sol (pregel solution), a trace amount of fluorescent probe particles is mixed so that upon gelation the particles segregate into pores of the

Received: July 6, 2016
Accepted: December 5, 2016
Published: December 8, 2016

DOI: 10.1021/acsnano.6b04468
ACS Nano 2017, 11, 204−212

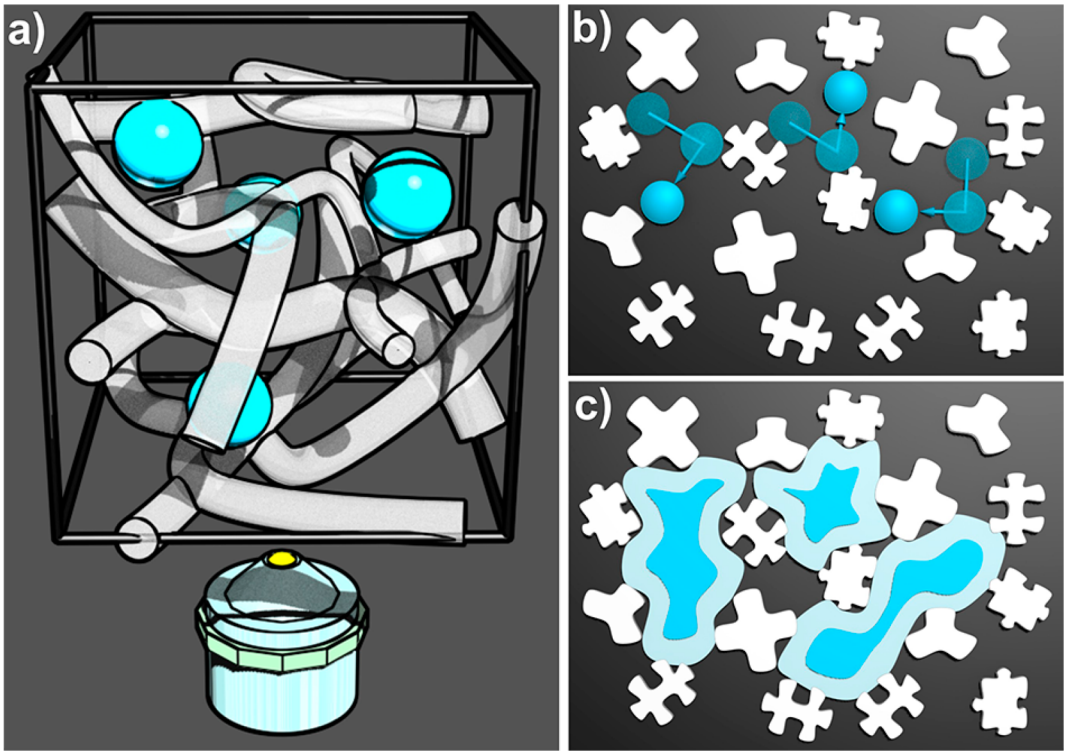

Figure 1. Key idea of this experiment. (a) Spherical probe particles (blue spheres) are embedded in a hydrogel porous network (gray sausages), and the spaces they explore are tracked as the particles diffuse by Brownian motion. (b) In this schematic 2D (2-dimensional) projection, 2D probe disks representing spherical probe particles (blue) diffuse by Brownian motion between randomly positioned, irregularly shaped spatial obstacles that represent gel porosity (white objects). Arrows denote schematically the time dependence of probe diffusion from one spatial spot to others. (c) In the projected two dimensions represented in this figure, the spatial areas traversed by Brownian motion of the probe particles (blue areas) and their contours in 2D space convoluted by particle radius (light blue areas) are followed schematically in real-space as time elapses.

resulting gel (Figure 1a). These particles were previously coated by BSA (bovine serum albumin), a strategy known to minimize specific adsorption.[15] The samples are mounted on a fluorescence microscope (the objective in Figure 1a), allowing particle trajectories to be recorded in the imaging plane. For the setup in which these ideas were tested as described below, the spatial resolution was ~10 nm and the time resolution was 10 ms.[27]

RESULTS AND DISCUSSION

Pore Size Distribution. Agarose hydrogel, which has widespread technological applications,[28,29] was selected as the test system in which to evaluate usefulness of this method. At high temperature, it is known that agarose dissolves in water, but upon cooling below this melting temperature, individual molecules assemble into helices to give supercoiled bundles and fibers, which further aggregate into 3D gel structures with channels and pores. To embed tracers into the gel, we mixed particles of appropriate surface chemistry and sizes (see detailed discussion in the following subsections) with agarose solution at high temperature and then quenched the mixture to room temperature. As the porous structure formed, these particles became caged within pores.

Typical trajectories of 500 nm radius particles in 0.25 wt % agarose gel are shown in Figure 2a. Within a few seconds of Brownian motion, the particles moved around the pores that they inhabited but remained within them. Since these particle trajectories were strictly restricted to well-defined pores, as in the scheme depicted in Figure 1c, the pore size is defined here as the sum of trajectory radius and particle radius, in which the former is the average distance from each point to the trajectory mass center. Experiments in this real hydrogel system showed that whereas the measurements within a given pore were highly repeatable, the pores themselves were polydisperse, from 0.5 to 1.5 μm in radius, with irregular shape.

Data of this kind gave the pore size distributions summarized in Figure 2b for the agarose concentrations 0.25, 0.50, and 0.75 wt %. With increasing agarose concentration, the peak pore size decreased (520 and 250 nm for 0.50 and 0.75 wt %, respectively) and the pore size distribution narrowed (power−law-like distribution for 0.25 wt %, Gaussian-like distribution for 0.50 and 0.75 wt %, with widths 200 and 80 nm, respectively). These trends, consistent with previous NMR and turbidity measurements by others,[30−32] confirm that this particle-tracking-based method can reliably characterize agarose gel structure.

In the Supporting Information, Figure S2 presents detailed comparison to pore sizes in agarose gel inferred previously from other methods: AFM,[33] electrophoresis,[34] FCS,[35] FRAP,[36] NMR,[30] and turbidity.[31,32] All of these literature data sets follow a trend qualitatively consistent with the power−law decay that we also find, but the exact values vary systematically from one method to another. Our data are quantitatively consistent with findings from NMR[30] and turbidity[31,32] and fall in the middle ground between findings from the other methods. We consider that differences between these literature findings might stem in part from some systematic difference inherent to those methods but might also be influenced by the fact that the

DOI: 10.1021/acsnano.6b04468
ACS Nano 2017, 11, 204−212

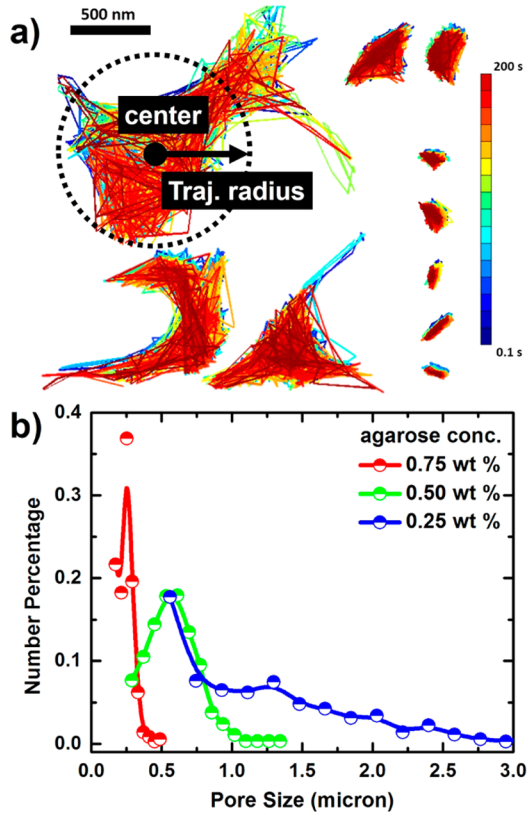

Figure 2. Pore size distribution probed by particle tracking. (a) Typical time-lapse trajectories of BSA-coated 500 nm radius latex particles in 0.25 wt % agarose gel. To compare trajectories, trajectory radius indicated in this panel is defined as the average distance from each point to the trajectory mass center. The trajectories are color-coded according to time as specified on the right. (b) Pore size distribution for various agarose concentrations obtained from about 500 trajectories of probe particles in each instance. The blue, green, and red points denote 0.25, 0.50, and 0.75 wt % gel, as probed by 500, 250, and 100 nm radius particles, respectively.

pore size of agarose gels is known to depend on the cooling history, which varied among these studies.

Testing Limits of the Method. To select a particle surface chemistry that would prevent specific binding to the agarose fibers, we tested four options: latex particles that were chemically modified with carboxyl, amine, and sulfate groups and carboxyl-modified particles to which BSA was allowed to adsorb. The first three displayed a strong tendency to permanently bind to the gel network, probably interacting with the −OH groups of agarose, but the last did not, showing the BSA-impeded adsorption (Figure S1).

We now turn to weak but long-range interactions such as electrostatic repulsion between the particles and the gel framework, which in principle might slow particle diffusion and prevent them from fully exploring the pores. Consider hypothetical probe particles with sizes much smaller than the pore size and with surface chemistry totally inert to the pore framework. One would expect such particles to diffuse freely at short times as if suspended only in solvent, but if the particle surface chemistry caused them to interact with the pore, diffusion would be slowed. Following this consideration, we embedded 50 nm radius BSA-coated particles into 0.25 wt % agarose gels. As shown in Figure 3a, the trajectories were quite extended, suggesting that the particles were small enough to explore from pore to pore. In Figure 3b, the corresponding mean square displacement, MSD, is plotted against time, *t*. The MSD curve agrees at early times with expectation for free-diffusion for the first few points (the black line), but then deviates from it, indicating unhindered and hindered diffusion at short and long times, respectively. By fitting the first few points to MSD = 4*Dt*, where *D* is the diffusivity, we obtain D = 3.1 $\mu m^2/s$, which is close to the value in pure water (4 $\mu m^2/s$). Therefore, we conclude that long-ranged interactions between the BSA-coated particles and the agarose gel framework were minimal.

It is reasonable to inquire whether the presence of particles themselves modified the structure of these gels as they formed. From the following points of view, it is unlikely to be a major influence. First, the probe particle concentration was low, ∼0.002 wt % particles to water (see the Methods). Second, the BSA-coated particles were, as shown above, inert with respect to the agarose network environment. Third, pore size distributions measured in this work are quantitatively

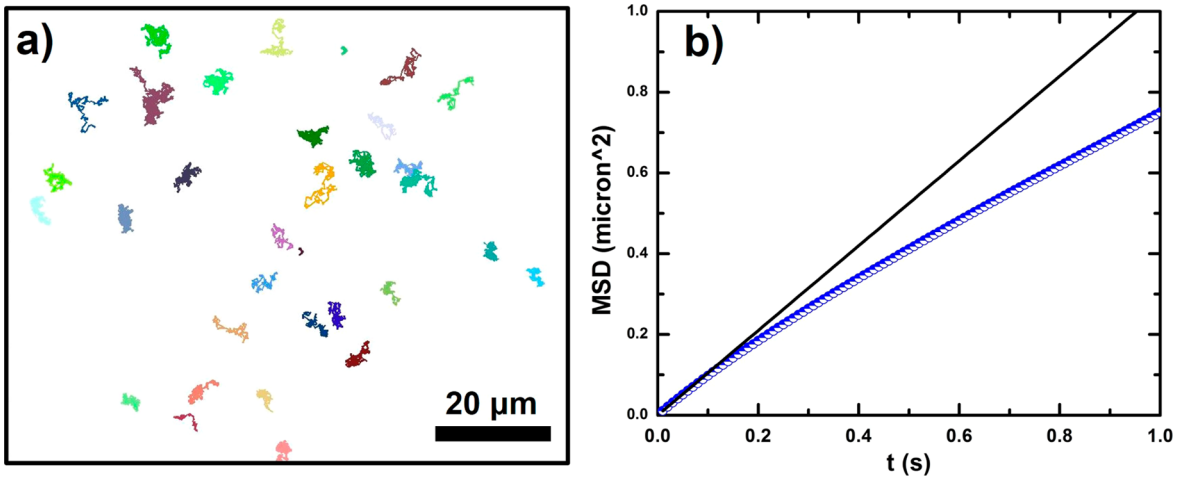

Figure 3. Diffusion of 50 nm radius particles in 0.25 wt % agarose gel. (a) Representative map of trajectories, *i.e.*, spatial position drawn as a function of elapsed time with colors that denote different trajectories. (b) Mean square displacement (MSD) plotted against time with the black line indicating free diffusion and slope unity.

DOI: 10.1021/acsnano.6b04468
ACS Nano 2017, 11, 204−212

comparable to literature results measured by NMR[30] and turbidity.[31,32] No direct evidence about this is available at this time, however.

Convolution with Probe Particle Size. Physically, it is clear that the displacement trajectories of tracer particles much smaller than individual pores cannot reveal the true sizes of individual pores, whereas larger particles can be trapped within individual pores without the chance of escape by Brownian motion. The size between pores determines the demarcation between these extremes. This notion, analogous to mesh size in polymer solutions, will likely be polydisperse in a random gel network. Probe particles smaller than the smallest pore opening can move from pore to pore, exploring the entire space (Figure 4a), but it is different for larger probe particles (Figure 4b).

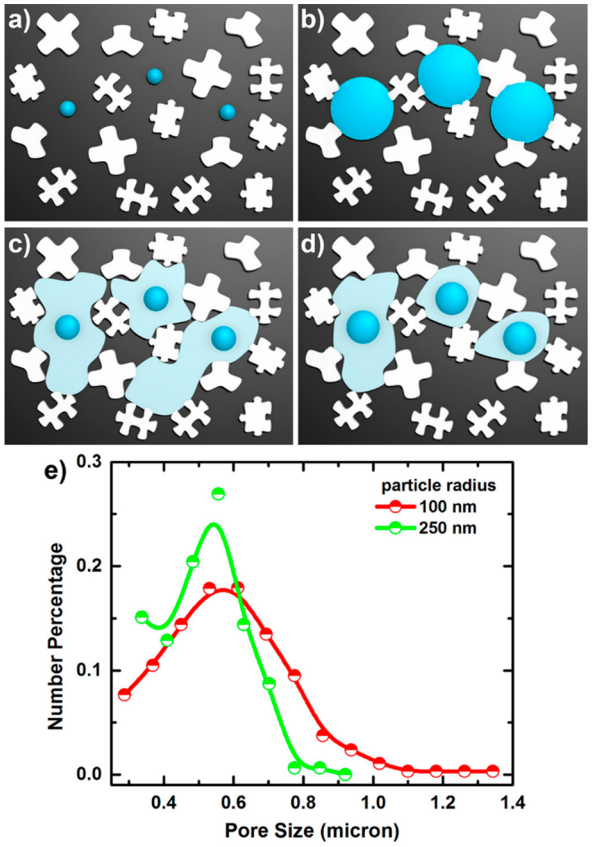

Figure 4. Effect of particle size on the measured pore size. (a–d) Probe disks (blue) move between hindering elements (white) with different probe sizes. The light blue areas mark the pore areas mapped out by this Brownian diffusion. (e) Pore size distribution inferred from 100 and 250 nm radius particles (red and green curves, respectively) in 0.5 wt % agarose gel.

Probes of intermediate size can explore a finite, nearby space, resulting in caged trajectories (Figure 4c,d). It is noteworthy that very small probe particles stand a chance of passing through multiple pore openings, which if not recognized in an experiment, would lead to inferring pore sizes larger than the actual ones (Figure 4c,d, right-most probe).

This anticipated scenario is confirmed by our measurements in 0.5 wt % agarose gel with 50, 100, 250, and 500 nm radius particles. The 50 nm particles are so small that most of them diffuse freely similar to the case shown in Figure 4, whereas the 500 nm particles are so large that most of them are nonmotile, so neither can be used to measure reliably the pore size distribution. The 100 and 250 nm radius particles of intermediate size report pore size distributions that are convoluted with particle radius (Figure 4e). Therefore, the pore size we infer is probe size dependent to some extent. For agarose gels studied here, we tested particles with different radii (from 50 to 500 nm) in different agarose concentrations and found that 250/500, 100/250, and 100 nm particles are appropriate for 0.25, 0.5, and 0.75 wt % agarose, respectively. Taken together, these considerations validate this method for gels in the stationary state before stimuli are applied to them.

Temperature Dependence. To test the capability of this method to capture stimulus response, we considered the temperature dependence of agarose hydrogel, which has been studied many times on the ensemble-averaged, macroscopic level.[37] Specifically, we selected 0.25 wt % agarose gel in a temperature range of 25−70 °C, which is below the known fully dissolving temperature ~90 °C. As shown in Figure 5a, the average pore size increased and its distribution narrowed during heating: the pores tended to become larger and more monodisperse. Enlarged pore size is expected from partial dissolution of agarose fibers. Narrowed distribution of pore size is rationalized by considering that the pore size distribution at the starting temperature of 25 °C was largely fixed by the original quenching kinetics and hence "overly" polydisperse, but that higher temperature favored a distribution closer to being thermodynamically determined and more monodisperse. Cooling from high temperature (Figure 5b) left the pore size distribution essentially unchanged. This large hysteresis agrees qualitatively with macroscopic measurements.[37,38] It is interesting and potentially useful to learn, from these real-space experiments, that heating/cooling cycles can narrow the pore size distribution.

An advantage of this particle tracking method is that it allows one to map how individual pores evolve with temperature. Illustrative examples are given in Figure 5c, where the trajectories for particles 1−3 are plotted at different temperatures during a single heating/cooling cycle. During heating, particle 1 experiences a gradual enlargement of the pore in which it sits. For particle 2, its pore remains unchanged up to 60 °C and then suddenly enlarges at 65 °C. The pore of particle 3 shows no detectable change throughout the entire heating range. These three particles are representative of three kinds of pore behavior in response to heating: gradual enlargement, sudden burst, and no change. On the other hand, cooling had little effect on measurement of individual particles or on the inferred pore size distribution data (Figure 5b).

Despite temperature dependence of the shapes and sizes of individual pores quantified by this method, centers of individual pores identified from particle trajectories varied little, but we did observe infrequent events where the whole trajectory of a particle drifted to a new position during heating (Figure 6a). From 60 to 70 °C, the trajectories of particles **i** and **k** hold the same position, whereas the trajectory of particle **j** moved to the upper right about 500 nm. These events suggest two possible underlying pore rearrangement mechanisms (Figure 6b,c). In Figure 6b, the hindering elements surrounding the moving particle are susceptible to heating (labeled by pink), and move more or less together to the right upon heating. As a result, the particle resides in the "old" pore but with a new position, but in Figure 6c, only one hindering element to the right of the particle responds to heating (labeled by pink) by dissolving partially to allow the probe particle to pass through it. However, in this example the pore happened to reform by recondensation

DOI: 10.1021/acsnano.6b04468
ACS Nano 2017, 11, 204−212

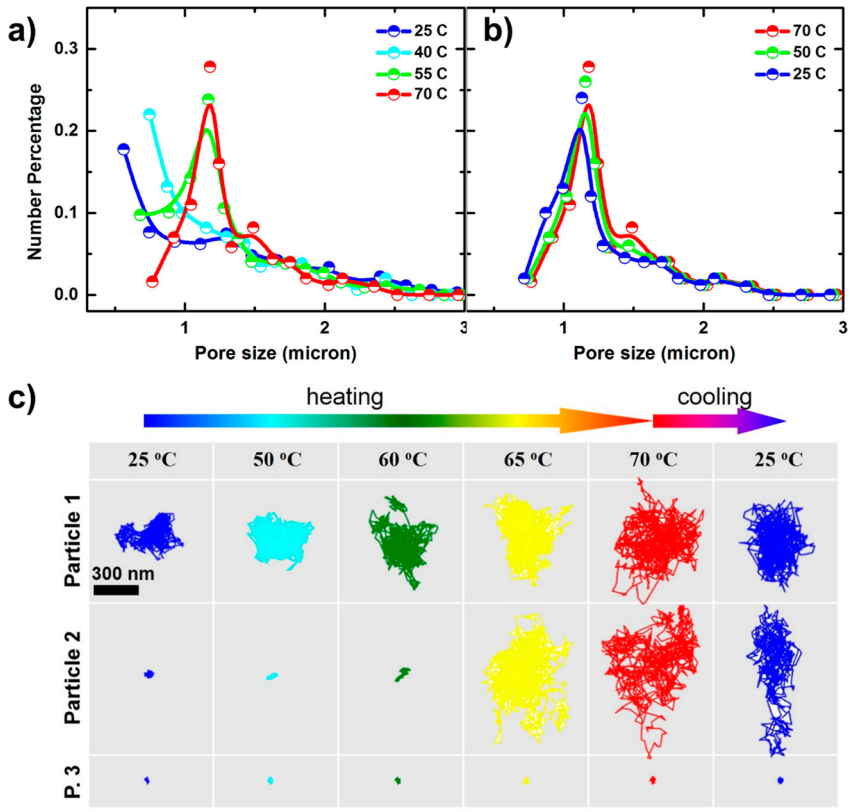

Figure 5. Response of pore-size distribution to temperature changes. (a) Pore size distributions of 0.25 wt % agarose gel upon heating with blue, teal, green, and red points corresponding to measurements at 25, 40, 55, and 70 °C, respectively, beginning at 25 °C. (b) Pore size distributions of 0.25 wt % agarose gel during cooling from 70 °C with red, green, and blue points corresponding to 70, 50, and 25 °C, respectively. (c) Typical pore behavior during a single heating/cooling cycle with rows corresponding to the identity of three representative particles and columns identifying temperature.

hence preventing the particle from returning, causing the particle to inhabit a "new" pore with a new position. The former mechanism is less likely as it requires a large-scale, collective structural rearrangement.

How Gel Microstructure Responds to Shear Deformation. For many technological applications, an essential mechanical property of gels is yield: beyond a certain stress or strain, the modulus drops dramatically.[39] In order to explore the accompanying microscopic structural changes, we developed a shear stage compatible with inverted microscopes (see the Methods for details) to track structural changes during shear by direct, *in situ* measurements following the same principle outlined above. Agarose gel of concentration 0.25 wt % was again selected for study, with findings summarized in Figure 7. For strains less than the yield point of 10% strain, the pore size distribution was essentially unchanged (Figure 7a), indicating that the gel structure remained intact, but larger strain caused a drastic change: a fraction of the particles were released from confining pores and subsequently underwent free Brownian motion or even some sort of "drifting-like" global flow (Figure 7b, the majority of the trajectories are unbounded), while the other fraction of the particles remained confined (Figure 7b, trajectories inside the dashed circle). Observations throughout the gel sample revealed that the released particles were usually spotted in large domains up to 100 μm in their 2D projection and that these domains were discontinuously distributed across the gel volume. We cannot define or measure "pore sizes" for the unbounded particles, but we can still do so for the bounded ones (Figure 7a, green and red curves). Quantification showed that the pore size distribution became less polydisperse. Its peak shifted toward smaller pores, and the pore size distribution became insensitive to strain after the sample was deformed beyond yield point.

To rationalize tentatively this observed strain-induced behavior, we postulate that the deformation beyond yield point changed the interconnectivity of gel pores. In the random fiber network arrangement sketched schematically in Figure 7c, the pore size is polydisperse and the fiber density is distributed nonuniformly. The pores in the top half are relatively large with low local fiber density, giving a relatively small mechanical strength whereas the pores in the bottom half are smaller. Although all the pores can withstand a small strain regardless of their size (Figure 7d), a large strain causes the large, weak pores to selectively rupture, releasing probes and appearing as "fractured" domains (Figure 7e). Since measurements of pore size distribution include data for intact pores only, it is understandable that the remnant pores are characterized by a narrower pore size distribution with a smaller peak, as we observed (Figure 7a).

CONCLUSION AND PERSPECTIVE

This paper has characterized the microstructure of agarose gel both on ensemble-averaged and single-pore levels by using fluorescence imaging to track the displacement trajectories of probe particles. We further extended this method to follow the gel's microstructural changes in response to environmental triggers of temperature and shear deformation. In comparison to traditional methods of pore size characterization in

DOI: 10.1021/acsnano.6b04468
ACS Nano 2017, 11, 204–212

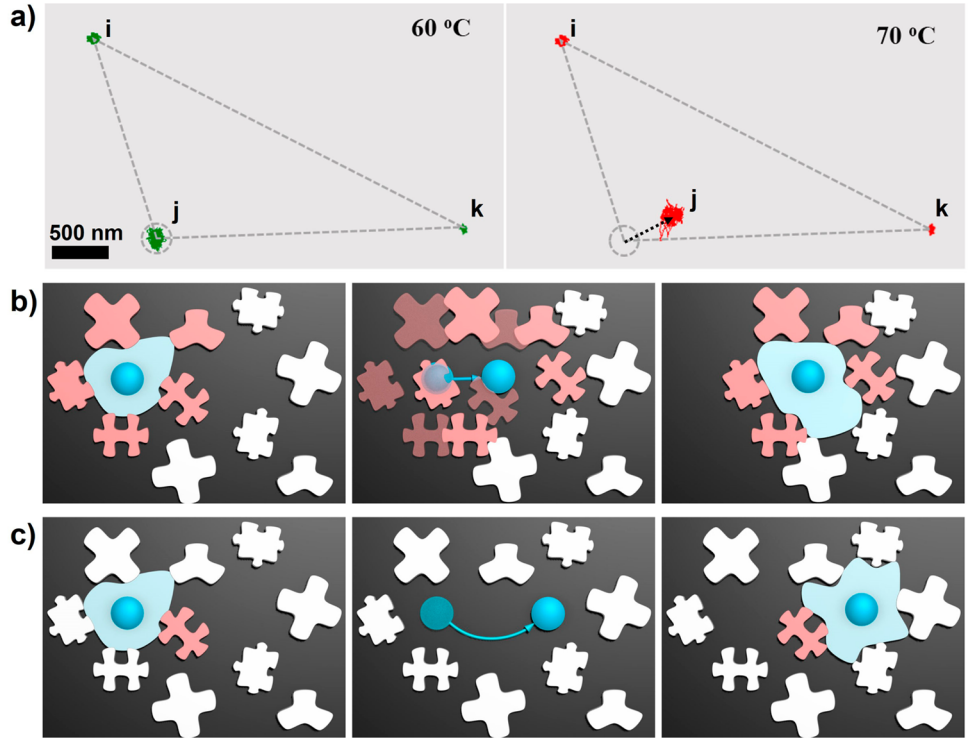

Figure 6. Pore rearrangements during heating. (a) Trajectories of three representative particles at 60 and 70 °C, in which particles i and k are held in position but particle j drifts to the upper right. Two possible mechanisms of pore rearrangement may account for this drift: (b) the large-scale, collective movement of hindering elements surrounding the particle and (c) the dissolving/recondensation of a "gate" hindering element. The heat-susceptible hindering elements are highlighted in pink.

hydrogels, the current method conveniently measures local/single-pore response, providing a detailed, microscopic perspective. It is envisioned that this method can be readily applied not only to the agarose system studied here but also to other recently developed "smart" gels that respond to a wide range of environmental triggers[40−42] to reveal the underlying structural responses.

We conclude with a frank evaluation of the experimental difficulties for those who might consider implementing this strategy to characterize pore size distribution in other experimental systems. One must carefully consider not only the probe particle's surface chemistry but also its size before attempting to employ this method in an unknown system. The probe surface chemistry must be inert to the gel framework so that the probe particle can effectively explore all of the porous space without modifying the gel structure, and its geometrical size must be moderately smaller than the pore size. For gel structures and the micron-sized pores considered in this study, one can use probes whose size is in the range of 100−1000 nm. For gel structures with nanometer-sized pores such as polyacrylamide gels, it would be necessary to switch to probes of smaller size, for example quantum dots or even probes composed of molecular dyes (~1 nm in dimension).

Although this paper emphasizes the promise of this method to characterize gel response to environmental triggers such as sudden switch of temperature and shear deformation, an additional challenge for those seeking to implement this method is that the needed temperature cell and shear stage demand home-built modification of what is available commercially for implementation on an optical microscope. The needed modifications to enable these measurements, however, are relatively simple.

METHODS

Materials. Agarose was purchased from Fisher (Pittsburgh, PA) (molecular biology grade, low electroendosmosis, gelation temperature 34.5−37.5 °C). Latex particles (radius: 50, 100, 250, and 500 nm, polydispersity 3−5%) dyed with Nile Red were purchased from Invitrogen (Carlsbad, CA). Bovine serum albumin (BSA) solution (30 wt % in saline) was purchased from Sigma-Aldrich (St. Louis, MO). BSA-coated particles were prepared by incubating untreated particles in 1 wt % BSA solution for 1 h to allow BSA to adsorb, followed by three centrifuging/washing cycles. A desired amount of solid agarose was weighted into a glass vial with deionized water. The mixture was heated to 90 °C to fully dissolve agarose, to which a trace amount of BSA-coated particles (~0.002 wt % particle/water) was added. Considering the known fact that BSA is ultimately stable after exposure at long time up to only 70 °C,[43] we immediately quenched the solution to 70 °C to minimize BSA denaturation. Then the solution was cooled to 25 °C at a rate of 10 °C/min.

Imaging and Tracking. Observations were made using an epifluorescence microscope (Zeiss Observer Z1) with an EMCCD camera (Andor iXon). We visualized the diffusion of probe particles using a 100× oil objective focused deeply into the sample (>20 μm) to avoid potential wall effects. Video images were collected typically at 10−100 fps for 200 s and then analyzed. The particle tracking codes we used are standard in the colloid field (http://site.physics.georgetown.edu/matlab/) with refinements described in previous publications from this research group.[25,27] In each trajectory, the center of each particle was located in each time frame with 10 nm precision.

Temperature Control To Explore Response to Environmental Temperature Trigger. The temperature of the chamber stage was controlled with 0.1 °C precision using a controller purchased from Instec (TSA02i Inverted Microscope Thermal Stage) and home-machined to fit securely onto the epifluorescence microscope.

Shear Stage To Explore Response to Environmental Shear Trigger. The layout of the shear stage is shown in Figure 8. Designed to be compact (dimensions 18 × 12 × 8 cm) and lightweight, it could

DOI: 10.1021/acsnano.6b04468
ACS Nano 2017, 11, 204−212

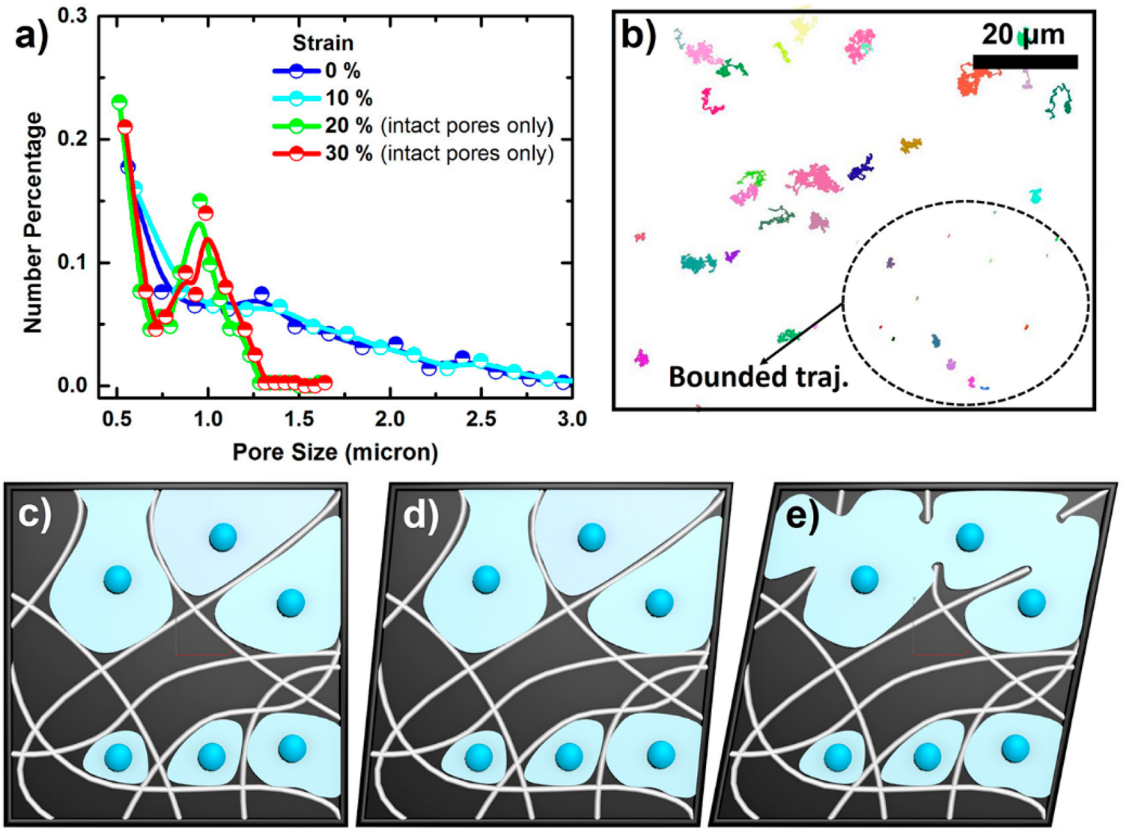

Figure 7. Pore size distribution after deformations beyond yield. (a) Pore size distribution probed by 500 nm radius particles in 0.25 wt % agarose gel at various strain amplitudes (blue, 0%; teal, 10%; green, 20%; red, 30%). Beyond yield, the largest pores disappeared and the pore size distribution retained only the intact pores, which were smaller. (b) Typical trajectories in a view at 20% strain. The majority of the trajectories are no longer bounded in space, but the minority of them (those inside the dashed circle) remain tightly bounded. A schematic 2D fiber network is subjected to increasing strains: (c) no strain, (d) small strain, for which this gel network deforms but does not yield, and (e) large strain, for which the top-half network with lower fiber density is damaged and the probe particles therein become unbounded regarding the space explored by their diffusion, whereas the bottom-half network with higher fiber density remains intact.

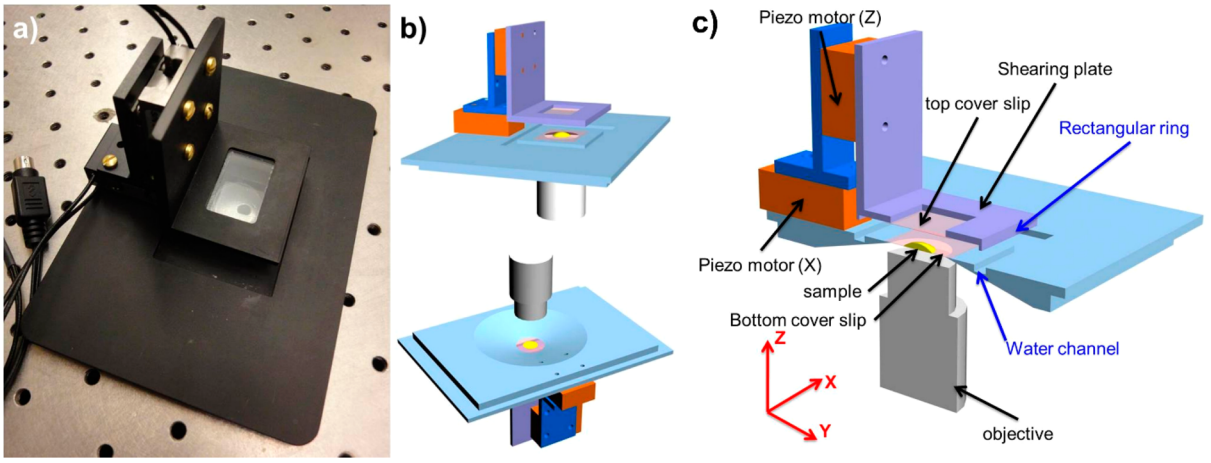

Figure 8. Layout of the home-built shear stage designed for *in situ* microscopic observation. (a) Photograph of the shear stage (dimensions 18 × 12 × 8 cm). (b) Top and bottom perspectives. The cone-shaped bottom of the stage features a large working area for oil immersion objectives. (c) Cross section of the stage with various functional parts indicated.

be easily mounted onto the stage of an inverted microscope (see Figure 8a,b for top and bottom views). The design requirements were that the unit be free of vibration and that it should allow parallel shear with constant gap between two solid surfaces with a stable, vibration-free displacement motor. To implement this, the samples were sheared between a top glass slide and a bottom coverslip (Figure 8c). The glass slide and coverslip were attached to the metal frame of the platform by soft paper glue, cut to size, and shaped to the needed size before use. This served not only to fix the glass plates but also, more importantly, to absorb height fluctuations that adventitious dust particles might otherwise introduce. The bottom plate, a thin coverslip (no. 1, 0.15 mm thick), was compatible with the short working distance of oil immersion microscope objectives. The surfaces of the two glass plates were modified with polyethylene glycol (PEG) to render the surface

DOI: 10.1021/acsnano.6b04468
ACS Nano 2017, 11, 204−212

inert and with colloidal particles to increase the roughness of the surface to discourage wall slip during shear.

Keeping the bottom coverslip immobile and close to the microscope objective, we sheared the top plate using two translation piezo stepper motors (Newport, Model AG-LS25). These piezo motors were chosen for their wide dynamic range, long stroke length, high precision, and minimal vibration. The *Z*-direction piezo motor was used to set the gap of the shear cell to be 50−200 μm. In this setup, the *X*-direction piezo motor can shear the top glass slide with a strain range between 0.002 and 400 at a steady shear rate up to 5 s^{-1} with a maximum resistance force of 2 N. To minimize solvent evaporation during the experiments, a channel surrounding the sample is filled with water, and then a rectangular metal ring is lowered to be immersed into the water, thus creating an airtight sample cell (Figure 8c).

ASSOCIATED CONTENT

Supporting Information

The Supporting Information is available free of charge on the ACS Publications website at DOI: 10.1021/acsnano.6b04468.

Comparison of the diffusion behavior of the BSA-coated and bare particles in agarose gels (Figure S1) and comparison of agarose gel pore sizes measured by different methods (Figure S2) (PDF)

AUTHOR INFORMATION

Corresponding Author

*E-mail: sgranick@ibs.re.kr.

ORCID

Steve Granick: 0000-0003-4775-2202

Author Contributions

L.J. and S.G. conceived the experiment; L.J. performed the measurements; L.J. and S.G. discussed the results and wrote the manuscript.

Notes

The authors declare no competing financial interest.

ACKNOWLEDGMENTS

We acknowledge support from the Dow Chemical University Research Program with the University of Illinois. At the IBS Center for Soft and Living Matter, S.G. acknowledges support by the Institute for Basic Science, Project Code IBS-R020-D1.

REFERENCES

(1) Wong, P. Z. *Methods of the Physics of Porous Media*; Academic Press, Inc.: San Diego, 1999.

(2) Gregg, S. J.; Sing, K. S. W. *Adsorption, Surface Area and Porosity*, 2nd ed.; Academic Press: San Diego, 1982.

(3) Richter, S.; Matzker, R.; Schroter, K. Gelation Studies, 4. Why do ″Classical″ Methods like Oscillatory Shear Rheology and Dynamic Light Scattering for Characterization of the Gelation Threshold Sometimes Not Provide Identical Results Especially on Thermoreversible Gels? *Macromol. Rapid Commun.* **2005**, *26*, 1626−1632.

(4) Djabourov, M.; Clark, A. H.; Rowlands, D. W.; Ross-Murphy, S. B. Small-Angle X-Ray Scattering Characterization of Agarose Sols and Gels. *Macromolecules* **1989**, *22*, 180−188.

(5) Pluen, A.; Netti, P. A.; Jain, R. K.; Berk, D. A. Diffusion of Macromolecules in Agarose Gels: Comparison of Linear and Globular Configurations. *Biophys. J.* **1999**, *77*, 542−552.

(6) Strange, J. H.; Rahman, M.; Smith, E. G. Characterisation of Porous Solids by NMR. *Phys. Rev. Lett.* **1993**, *71*, 3589−3591.

(7) Estroff, L. A.; Leiserowitz, L.; Addadi, L.; Weiner, S.; Hamilton, A. D. Characterization of an Organic Hydrogel: A Cryo-Transmission Electron Microscopy and X-ray Diffraction Study. *Adv. Mater.* **2003**, *15*, 38−42.

(8) Deng, W.; Yamaguchi, H.; Takashima, Y.; Harada, A. A Chemical-Responsive Supramolecular Hydrogel from Modified Cyclodextrins. *Angew. Chem.* **2007**, *119*, 5236−5239.

(9) Jiang, L. X.; Yan, Y.; Huang, J. B. Zwitterionic Surfactant/Cyclodextrin Hydrogel: Microtubes and Multiple Responses. *Soft Matter* **2011**, *7*, 10417−10423.

(10) Lee, K. Y.; Mooney, D. J. Hydrogels for Tissue Engineering. *Chem. Rev.* **2001**, *101*, 1869−1879.

(11) Stuart, M. A. C.; Huck, W. T. S.; Genzer, J.; Mueller, M.; Ober, C.; Stamm, M.; Sukhorukov, G. B.; Szleifer, I.; Tsukruk, V. V.; Urban, M.; Winnik, F.; Zauscher, S.; Luzinov, I.; Minko, S. Emerging Applications of Stimuli-Responsive Polymer Materials. *Nat. Mater.* **2010**, *9*, 101−113.

(12) Vermonden, T.; Censi, R.; Hennink, W. E. Hydrogels for Protein Delivery. *Chem. Rev.* **2012**, *112*, 2853−2888.

(13) Lin, C.-C.; Metters, A. T. Hydrogels in Controlled Release Formulations: Network Design and Mathematical Modeling. *Adv. Drug Delivery Rev.* **2006**, *58*, 1379−1408.

(14) Kim, S.-H.; Kim, J. W.; Kim, D. H.; Han, S.-H.; Weitz, D. A. Polymersomes Containing a Hydrogel Network for High Stability and Controlled Release. *Small* **2013**, *9*, 124−131.

(15) Valentine, M. T.; Perlman, Z. E.; Gardel, M. L.; Shin, J. H.; Matsudaira, P.; Mitchison, T. J.; Weitz, D. A. Colloid Surface Chemistry Critically Affects Multiple Particle Tracking Measurements of Biomaterials. *Biophys. J.* **2004**, *86*, 4004−4014.

(16) Kotlarchyk, M. A.; Botvinick, E. L.; Putnam, A. J. Characterization of Hydrogel Microstructure Using Laser Tweezers Particle Tracking and Confocal Reflection Imaging. *J. Phys.: Condens. Matter* **2010**, *22*, 194121.

(17) Wang, B.; Anthony, S. M.; Bae, S. C.; Granick, S. Anomalous yet Brownian. *Proc. Natl. Acad. Sci. U. S. A.* **2009**, *106*, 15160−15164.

(18) Li, W.; Liu, R.; Wang, Y.; Zhao, Y.; Gao, X. Temporal Techniques: Dynamic Tracking of Nanomaterials in Live Cells. *Small* **2013**, *9*, 1585−1594.

(19) Chen, Q.; Smith, J. M.; Park, J.; Kim, K.; Ho, D.; Rasool, H. I.; Zettl, A.; Alivisatos, A. P. 3D Motion of DNA-Au Nanoconjugates in Graphene Liquid Cell Electron Microscopy. *Nano Lett.* **2013**, *13*, 4556−4561.

(20) Crocker, J. C.; Valentine, M. T.; Weeks, E. R.; Gisler, T.; Kaplan, P. D.; Yodh, A. G.; Weitz, D. A. Two-Point Microrheology of Inhomogeneous Soft Materials. *Phys. Rev. Lett.* **2000**, *85*, 888−891.

(21) Valentine, M. T.; Kaplan, P. D.; Thota, D.; Crocker, J. C.; Gisler, T.; Prud'homme, R. K.; Beck, M.; Weitz, D. A. Investigating the microenvironments of inhomogeneous soft materials with multiple particle tracking. *Phys. Rev. E: Stat. Phys., Plasmas, Fluids, Relat. Interdiscip. Top.* **2001**, *64*, 061506.

(22) Savin, T.; Doyle, P. S. Statistical and sampling issues when using multiple particle tracking. *Phys. Rev. E* **2007**, *76*, 021501.

(23) Larsen, T. H.; Furst, E. M. Microrheology of the liquid-solid transition during gelation. *Phys. Rev. Lett.* **2008**, *100*, 146001.

(24) Rich, J. P.; McKinley, G. H.; Doyle, P. S. Size Dependence of Microprobe Dynamics During Gelation of a Discotic Colloidal Clay. *J. Rheol.* **2011**, *55*, 273−299.

(25) Anthony, S.; Hong, L.; Kim, M.; Granick, S. Single-Particle Colloid Tracking in Four Dimensions. *Langmuir* **2006**, *22*, 9812−9815.

(26) Crocker, J. C.; Grier, D. G. Methods of Digital Video Microscopy for Colloidal Studies. *J. Colloid Interface Sci.* **1996**, *179*, 298−310.

(27) Anthony, S.; Zhang, L.; Granick, S. Methods to Track Single-Molecule Trajectories. *Langmuir* **2006**, *22*, 5266−5272.

(28) Serwer, P. Agarose Gels: Properties and Use for Electrophoresis. *Electrophoresis* **1983**, *4*, 375−382.

(29) Normand, V.; Lootens, D. L.; Amici, E.; Plucknett, K. P.; Aymard, P. New Insight into Agarose Gel Mechanical Properties. *Biomacromolecules* **2000**, *1*, 730−738.

(30) Chui, M. M.; Phillips, R. J.; Mccarthy, M. J. Measurement of the Porous Microstructure of Hydrogels by Nuclear Magnetic Resonance. *J. Colloid Interface Sci.* **1995**, *174*, 336−344.

(31) Aymard, P.; Martin, D. R.; Plucknett, K.; Foster, T. J.; Clark, A. H.; Norton, I. T. Influence of thermal history on the structural and mechanical properties of agarose gels. *Biopolymers* **2001**, *59*, 131−144.
(32) Narayanan, J.; Xiong, J. Y.; Liu, X. Y. (2006). Determination of Agarose Gel Pore Size: Absorbance Measurements vis a vis Other Techniques. *J. Phys.: Conf. Ser.* **2006**, *28*, 83−86.
(33) Pernodet, N.; Maaloum, M.; Tinland, B. Pore Size of Agarose Gels by Atomic Force Microscopy. *Electrophoresis* **1997**, *18*, 55−58.
(34) Slater, G. W.; Rousseau, J.; Noolandi, J.; Turmel, C.; Lalande, M. Quantitative Analysis of the Three Regimes of DNA Electrophoresis in Agarose Gels. *Biopolymers* **1988**, *27*, 509−524.
(35) Fatin-Rouge, N.; Starchev, K.; Buffle, J. Size Effects on Diffusion Processes within Agarose Gels. *Biophys. J.* **2004**, *86*, 2710−2719.
(36) Tinland, B.; Pernodet, N.; Weill, G. Field and Pore Size Dependence of the Electrophoretic Mobility of DNA: a Combination of Fluorescence Recovery after Photobleaching and Electric Birefringence Measurements. *Electrophoresis* **1996**, *17*, 1046−1051.
(37) Aymard, P.; Martin, D. R.; Plucknett, K.; Foster, T. J.; Clark, A. H.; Norton, I. T. Influence of Thermal History on The Structural and Mechanical Properties of Agarose Gels. *Biopolymers* **2001**, *59*, 131−144.
(38) Ishikiriyama, K.; Sakamoto, A.; Todoki, M.; Tayama, T.; Tanaka, K.; Kobayashi, T. Pore Size Distribution Measurements of Polymer Hydrogel Membranes for Artificial Kidneys Using Differential Scanning Calorimetry. *Thermochim. Acta* **1995**, *267*, 169−180.
(39) van Oosten, A. S.; Galie, P. A.; Janmey, P. A. Mechanical Properties of Hydrogels. In *Gels Handbook*; World Scientific, 2001; pp 67−79.
(40) Samchenko, Y.; Ulberg, Z.; Korotych, O. Multipurpose Smart Hydrogel Systems. *Adv. Colloid Interface Sci.* **2011**, *168*, 247−262.
(41) Harada, A.; Kobayashi, R.; Takashima, Y.; Hashidzume, A.; Yamaguchi, H. Macroscopic Self-Assembly Through Molecular Recognition. *Nat. Chem.* **2011**, *3*, 34−37.
(42) Appel, E. A.; Loh, X. J.; Jones, S. T.; Biedermann, F.; Dreiss, C. A.; Scherman, O. A. Ultrahigh-Water-Content Supramolecular Hydrogels Exhibiting Multistimuli Responsiveness. *J. Am. Chem. Soc.* **2012**, *134*, 11767−11773.
(43) Michnik, A. Thermal Stability of Bovine Serum Albumin DSC Study. *J. Therm. Anal. Calorim.* **2003**, *71*, 509−519.

DOI: 10.1021/acsnano.6b04468
ACS Nano 2017, 11, 204−212